Middle East Journal of Applied Science & Technology (MEJAST)
Volume 6, Issue 2, Pages 105-117, April-June 2023

Seismic Attributes for Enhanced Structural and Stratigraphic Interpretation in Onshore Fuba field, Niger Delta, Nigeria

U. Ochoma*

Department of Physics, Rivers State University, P.M.B 5080, Port Harcourt, Nigeria.
*Email: umaocho@gmail.com**

DOI: https://doi.org/10.46431/MEJAST.2023.6213

Article Received: 10 April 2023 *Article Accepted: 25 May 2023* *Article Published: 12 June 2023*

ABSTRACT

Seismic attributes for enhanced structural and stratigraphic interpretation of Fuba Field, Onshore Niger Delta, Nigeria using Well-log and 3D Seismic data are here presented. Well-to-Seismic ties, faults and horizon mapping, time-surface generation, depth conversion and seismic attributes generation were carried out using Petrel software. The structural interpretation of seismic data reveal highly synthetic and antithetic faults which are in line with faults trends identified in the Niger Delta. Of the 29 interpreted faults, only synthetic and antithetic faults are regional, running from the top to bottom across the field. These faults play significant roles in trap formation at the upper, middle and lower sections of the field. Two distinct horizons were mapped. Fault and horizon interpretation reveal closures which are collapsed crestal structures bounded by these two major faults. The depth structure maps reveal anticlinal faults. Reservoirs are found at a shallower depth from 6500 to 7500ft and at a deeper depth ranging from 11500 to 13000ft. The synthetic and antithetic faults act as good traps for the hydrocarbon accumulation in the study area. The variance and chaos values range from 0.0 to 1.0. The dip magnitude and azimuth values range from 0 to 90 degrees and 0 to 360 degrees. The variance edge, chaos, dip magnitude and azimuth analysis were used to delineate the prominent and subtle faults in the area. The results of spectral decomposition at a frequency of 12-35Hz indicates areas of low frequency and high amplitude associated with known hydrocarbon zones, the presence of channels, lobes and small scale faults in the field. The result of the seismic attribute analysis has shown that the Fuba field has good hydrocarbon prospects.

Keywords: Growth faults, Variance method, Chaos, Spectral decomposition, Niger Delta, Nigeria.

1.0. Introduction

Seismic attributes are quantities of geometric, kinematic, dynamic, or statistical features obtained from seismic data (Liner, 2004; Oyeyemi, and Aizebeokhai, 2015; Adewoye, et al, 2015). Seismic attributes need to be integrated in some interpretations as they can be used as tools for predicting reservoir geometry and possibly displaying lateral changes in thickness including fluid contacts (Steiner, and Lockhart, 1988). The geometrical seismic attributes can enhance the visibility of the geometrical characteristics of seismic events and are sensitive to the lateral variation of azimuth, continuity, similarity, curvature, energy, and dip (Adetokunbo, et al, 2016). Structural and stratigraphic traps could be very subtle and are therefore difficult to map accurately. The geometrical attributes are used for structural and stratigraphic interpretations of seismic data (Emujakporue, and Enyenilhi, 2020). It is therefore possible to use seismic attributes to map geological features such as faults (Ologe, and Olowokere, 2021).

Seismic attributes are extensively being used in the oil industry to predict subsurface reservoir properties (Srivastava et al, 2003). Several researchers have made enormous contributions based on seismic attributes for enhanced structural and stratigraphic interpretations within the Niger Delta basin to investigate the potentiality of hydrocarbon deposits (Ochoma, et al, 2023; Omoja and Obiekezie, 2019). Ochoma, et al, (2023) used the variance edge analysis to delineate the prominent and subtle faults in the area. The sweetness value ranges from 0 to 22,500. The high sweetness regions in the seismic data indicate high amplitude which indicates the presence of hydrocarbon-bearing sand units. The RMS amplitude values range from 0 to 13,000 in the reservoirs. The root mean square amplitude analysis also indicates the presence of hydrocarbon in seismic data. The relative acoustic impedance analysis was used for delineating lithology variation in the seismic sections. Omoja and Obiekezie

(2019) involved systematic picking of faults and mapping of horizons/reservoir tops across seismic volume and extraction of seismic attributes. Structural analysis indicates the presence of down-to-basin footwall and hanging wall faults associated with roll over anticlines and horst-block (back-to-back fault). Generated time and depth structural maps from three reservoir intervals (D3100, D5000, and D9000) revealed the presence of fault dependent closure across the field. Analyses of relevant seismic attributes such as root-mean-square (RMS) amplitude, maximum amplitude, average energy amplitude, average magnitude amplitude, maximum magnitude attribute and standard deviation amplitude, which were applied on reservoir tops, revealed sections with bright spot anomalies. These amplitude anomalies served as direct hydrocarbon indicators (DHIs), unravelling the presence and possible hydrocarbon prospective zones. In addition, structural top maps show that booming amplitude is seen within the vicinity of fault closures, an indication that these hydrocarbon prospects are structurally controlled.

This study is taken from Fuba Field, Depobelt, Niger Delta, Nigeria. The ultimate deliverable of this study was seismic attributes for enhanced structural and stratigraphic interpretation of the area. The major components of this study are: (a) Well Correlation performed in order to determine the continuity of the reservoir sand across the field. (b) Seismic Interpretation which involves well-to-seismic ties, fault mapping, horizon mapping, time surface generation, depth conversion, attributes generation, structural and stratigraphic interpretation. This gives more insight into seismic attributes for enhanced structural and stratigraphic interpretation of the area.

2.0. Location and Geology of the Study Area

The proposed study area Fuba Field is located in the onshore Niger Delta region. Figure 1 shows the map of the Niger Delta region showing the study area. The Niger Delta lies between latitudes 4° N and 6° N and longitudes 3° E and 9° E (Whiteman, 1982).

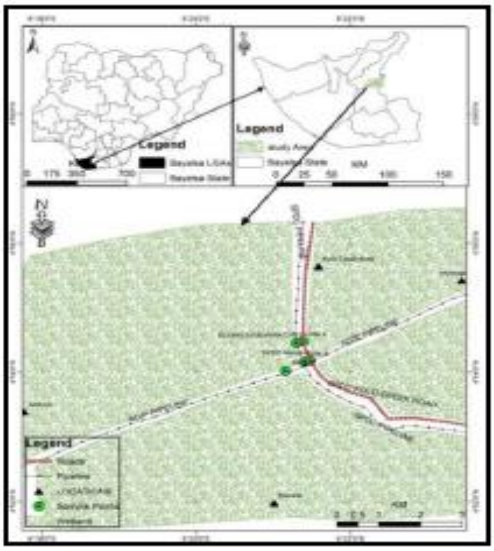

Figure 1. Map of Nigeria Showing the study Area, Fuba Field

The Delta ranks as one of the major oil and gas provinces globally, with an estimated ultimate recovery of 40 billion barrels of oil and 40 trillion cubic feet of gas (Adegoke et al., 2017). The coastal sedimentary basin of Nigeria has been the scene of three depositional cycles (Short and Stauble, 1967). The first began with a marine incursion in the middle Cretaceous and was terminated by a mild folding phase in Santonian time. The second included the growth

of a proto-Niger delta during the Late Cretaceous and ended in a major Paleocene marine transgression. The third cycle, from Eocene to Recent, marked the continuous growth of the main Niger delta. A new threefold lithostratigraphic subdivision is introduced for the Niger delta subsurface, comprising an upper sandy Benin Formation, an intervening unit of alternating sandstone and shale named the Agbada Formation, and a lower shaly Akata Formation. These three units extend across the whole delta and each ranges in age from early Tertiary to Recent. They are related to the present outcrops and environments of deposition. A separate member of the Benin Formation is recognized in the Port Harcourt area. It is Miocene-Recent in age with a minimum thickness of more than 6,000ft (1829m) and made up of continental sands and sandstones (>90%) with few shale intercalations (Horsfall et al., 2017). Subsurface structures are described as resulting from movement under the influence of gravity and their distribution is related to growth stages of the delta (Ochoma et al., 2020). Rollover anticlines in front of growth faults form the main objectives of oil exploration, the hydrocarbons being found in sandstone reservoirs of the Agbada Formation. The oil in geological structures in the basin may be trapped in dip closures or against a synthetic or antithetic fault.

3.0. Methodology

3.1. Well-Log and Seismic Data Quality Control

Well correlation involves lithologic description, picking top and base of sand-bodies, fluid discrimination and then linking these properties from one well to another based on similarity in trends. Correlation of reservoir sands was achieved using the top and base of reservoir sands picked. The correlation process was possible based on similarity in the behaviour of the gamma ray log. In the Niger Delta, the predominant lithologies are sands and shales. In order to discriminate between these two lithologies in the subsurface, the gamma ray log is used. After defining the lithologies, the resistivity log was used for discriminating the type of fluid occurring within the pores in the rocks.

There are seven basic steps involved in seismic interpretation relevant to this study and they include well-to-seismic ties, Fault Mapping, Horizon mapping, Time surface generation, velocity Modelling, Depth Conversion and generation of seismic attributes. The sonic log, which is the reciprocal of velocity, was calibrated using the checkshot data. The calibration process is necessary in order to improve the quality of the sonic log because the sonic log is prone to washouts and other wellbore related issues. The results of calibrating the sonic log with the checkshot gives the calibrated sonic log.

The calibrated sonic log is used along with the density log to generate an acoustic impedance (AI) log. The acoustic impedance log is calculated for each layer of rock. The next step involves generating the reflectivity coefficient (RC) log. The RC is calculated and generated using the AI log. The RC log generated is then convolved with a wavelet to generate a synthetic seismogram which is comparable with the seismic data. The statistical wavelet utilized for convolution is extracted from the seismic data. The synthetic seismogram was generated. The mathematical expressions that govern the entire well-to-seismic tie workflow are presented below:

$$AI = \rho v \quad (1)$$

$$RC = \frac{\rho_2 v_2 - \rho_1 v_1}{\rho_2 v_2 + \rho_1 v_1} \quad (2)$$

Synthetic Seismogram = $\frac{\rho_2 v_2 - \rho_1 v_1}{\rho_2 v_2 + \rho_1 v_1} * wavelet$ (3)

where AI = acoustic impedance, RC = reflection coefficient, ρ = density; v = velocity.

Faults were identified as discontinuities or breaks in the seismic reflections. Faults were mapped on both inline and cross-line directions. Horizons are continuous lateral reflection events that are truncated by fault lines. The horizon interpretation process was conducted along both inline and crossline direction. At the end of the horizon mapping, a seed grid is generated which serves as an input for time surface generation. Time surfaces were generated using the seed grids gotten from the horizon mapping process. The third order polynomial velocity model generated was used to depth convert the time surfaces of the reservoirs of interest.

3.2. Variance (Edge Detection) Method

The variance attribute is edge imaging and detection techniques. It is used for imaging discontinuity related to faulting or stratigraphy in seismic data. Variance attribute is proven to help in imaging of channels, fault zones, fractures, unconformities and the major sequence boundaries (Pigott. et al, 2013). In the Petrel software, the variance attribute uses an algorithm that computes the local variance of the seismic data through a multi-trace window with user-defined size. The local variance is computed from horizontal sub-slices for each voxel. A vertical window was used for smoothing the computed variance and the observed amplitude normalized. The variance attribute measures the horizontal continuity of the amplitude that is the amplitude difference of the individual traces from their mean value within a gliding CMP window.

$$\sigma^2 = \frac{1}{n}\sum_{f_i=1}^{n}(x_i + x_m)^2 \qquad (4)$$

Where $\sigma =$ standard deviation, $\sigma^2 =$ variance, $n =$ the number of observations, $f_i =$ frequency, $x_i =$ the variable, $x_m =$ mean of x_i

3.3. Chaos

Chaos attribute is defined as a measure of the “lack of organization” in the dip and azimuth estimation method. It can be used to distinguish different sediment facies in lithology variation environments (for example, sand and shale).

3.4. Dip magnitude and Azimuth

Dip magnitude is analogous to strike and dip of sedimentary layers. The dip magnitude is defined as the angle between the steepest direction of a plane and a horizontal plane, where values range from 0 to 90. The dip magnitude attribute computation in Petrel software makes use of the inbuilt formula:

$$\text{True dip} = \tan^{-1}\left(\frac{\tan(\theta_y)}{\tan(\beta_x)}\right) \quad (5)$$

where $\theta_y =$ apparent dip in a direction (y) and $\beta_x =$ dip azimuth relative to a direction (x).

Dip azimuth is the direction (relative to the north) that plane is dipping, where values range from 0 to 360. The dip azimuth attribute computation in Petrel software makes use of the inbuilt formula:

$$\beta_x = \tan^{-1}\left(\frac{\tan(\theta_x)}{\tan(\theta_y)}\right) \quad (6)$$

where θ_y = apparent dip in a direction (y), θ_x = apparent dip in a direction (x) and β_x = dip azimuth relative to a direction (x).

Dip magnitude and azimuth are good attributes, not only for showing overall structure folds, but can be used to identify faults with very small displacement.

3.5. Spectral Decomposition

Spectral decomposition is a frequency attribute. It involves separating and classifying seismic events within each trace based on their frequency content. Each 1D trace was decomposed from the time domain into its corresponding 2D representation in the time-frequency domain using algorithms. Once each trace was transformed into the time-frequency domain, a band-pass filter was applied to view the amplitude of seismic data at different frequencies.

The short-time Fourier transform (STFT) spectrogram which is the squared modulus of the STFT and the spectral energy density is defined as (Cohen, 1989)

$$SP_s(t, f) = /\int_{-\infty}^{\infty} s(\tau)h(\tau - t)e^{-j2\pi f\tau}d\tau /^2 \quad (7)$$

Where, $h(\tau - t)$ = the window function, $s(\tau)$ = the signal, SP_s = the short-time Fourier transform

j = the imaginary unit, τ = the time delay.

The relationships between the amplitude spectrum ($A(w)$) and the phase spectrum ($\gamma(w)$) of the estimated transformed signals are presented in equations 8 and 9

$$/A(w^T)/ = \sqrt{A_r + A_i} \quad (8)$$

$$\gamma(w) = \mathrm{Tan}^{-1}\left[\frac{A_i}{A_r}\right] \quad (9)$$

A_r = real part of $A(w^T)$, A_i = imaginary part of $A(w^T)$, w = frequency, T = transform of the signal and $A(w^T)$ = amplitude of transformed trace at frequency w.

4.0. Results and Discussion

4.1. Reservoir Identification, Correlation and Well-to-Seismic Ties

The results for lithology and reservoir identification are presented in (Figure 2). A total of nine sand bodies (A, B, C, D, E, F, G, H and I) were identified and correlated across all seven wells in the field. Two reservoir sands were selected for the purpose of this study (A and I). The resistivity logs which reveals the presence of hydrocarbons

were used to identify the hydrocarbon bearing sands. On (Figure 2), the sands are coloured yellow while shales are grey in colour. The results for well-to-seismic tie conducted on Fuba field using density log, sonic log and checkshot of Well-1 is presented in Figure 3. A statistical wavelet (ISIS time) was used to give a near perfect match between the seismic and synthetic seismogram.

4.2. Faults and Horizons Interpretation

The results for the interpreted faults in Fuba field are presented in Figure 4 shows both synthetic and antithetic faults interpreted along seismic inlines. Faults are more visible along the inline direction because this direction reveals the true dip position of geologic structures. The variance time slice was used to validate the interpreted faults as seen on Figure 5. All interpreted faults are normal synthetic and antithetic faults. A total of twenty-nine faults were interpreted across the entire seismic data. Of the 29 interpreted faults, only F1 (synthetic fault) and F16 (antithetic fault) faults are regional, running from the top to bottom across the field. Hence, these faults play significant roles in trap formation at the upper, middle and lower sections of the field. As can be seen from Figure 6, all drilled wells within the field are within the two major faults identified (F1 and F16 faults).

The results for the interpreted seismic horizons (Horizon A and Horizon I) are also presented in Figure 4. On these horizons, the fault polygons were generated and eliminated. The horizons were used as inputs for the generation of reservoir time surfaces.

The reservoir time surfaces (A and I reservoirs) reveal that the reservoir structure is a collapsed crest, bounded by two regional faults (F1 and F16). Reservoir A and I time surfaces are truncated by two bounding faults and three minor inter-reservoir faults. The similarity in structure identified on reservoirs A and I reveals that the field is structurally controlled by faults.

4.3. Depth Surfaces

The result of depth conversion residual analysis is presented in Table 1. The depth residual is the difference between the depth values of the well top from each well and the depth value from the depth converted reservoir surfaces. The depth residual analysis revealed that surfaces converted using the linear velocity function had the largest residuals ranging from -31.60 to +61.67 and from -50.58 to +40.84ft in reservoir A and reservoir I respectively. This is closely followed by the residual values obtained with the 2^{nd} order polynomial function. The third order polynomial function shows the least residuals, ranging from -6.69 to +6.61 ft in reservoir A, and -9.48 to +8.42ft respectively. The negative depth residual indicates that the depth conversion process displaces the reservoir to a greater depth than where it occurs in the subsurface, while a positive depth residual signifies that the depth converted result has placed the reservoir at a shallower depth (Ogbamikhumi and Aderibigbe, 2019). The resultant depth residual values generated using the various velocity models (linear, 2^{nd} and 3^{rd} order polynomials) were compared in order to select the most suitable velocity model for depth conversion of the reservoir surfaces. Figure 7 shows the 3^{rd} order polynomial velocity model which was selected and used as most suitable velocity model for converting A and I reservoirs from time to depth because it has the least residuals. The depth converted reservoir A and I surfaces are presented in Figures 8 and 9 for the third order polynomial velocity function. The depth structure maps reveal that the reservoirs are anticlinal and fault supported. Reservoir A is found at a shallower depth from

6500 to 7500 ft while reservoir I is found at a deeper depth ranging from 11500 to 13000ft respectively. The depth residuals recorded from the various well locations were used to generate depth residual maps which are presented in Figures 10 and 11 respectively. The depth residual maps revealed that higher residuals on reservoir A and I surfaces are associated with the eastern and western regions which are areas not penetrated by any well.

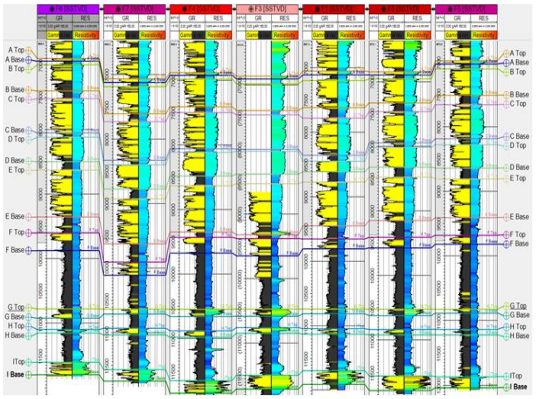

Figure 2. Well Section Showing Reservoir Identified and Correlated Across Fuba Field

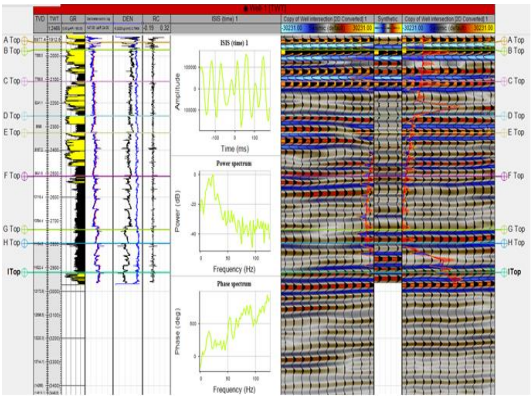

Figure 3. Synthetic Seismogram Generation and Well-to-seismic Tie Conducted for Fuba Field using Well-1 Checkshot

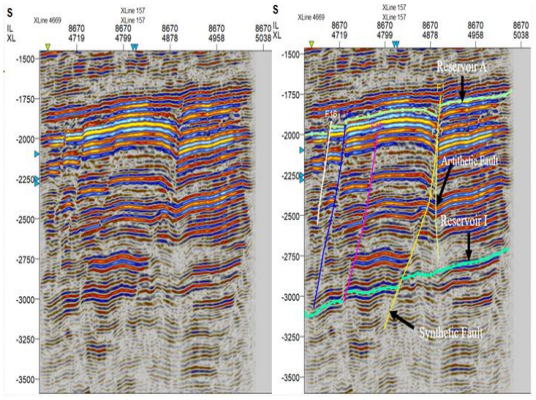

Figure 4. Faults and Horizons Interpreted Along Seismic section (a) Original Seismic, and (b) Faults and Horizons Interpreted

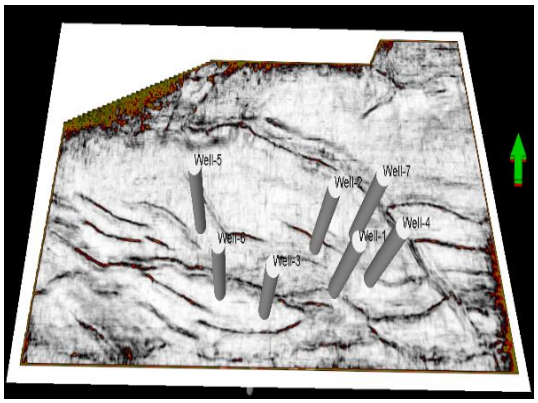

Figure 5. Variance Attribute Generated Inline Showing Clearly Resolved Faults on Time Slice

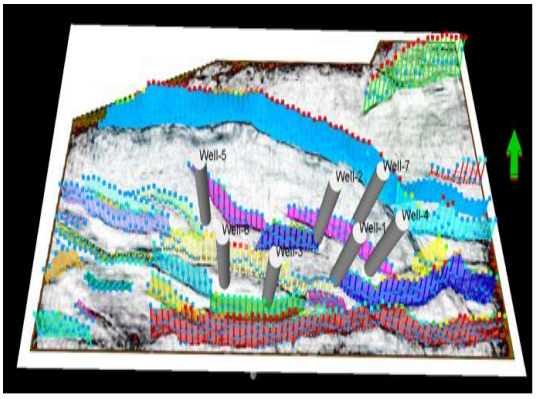

Figure 6. Interpreted Faults Displayed on the Variance Time Slice

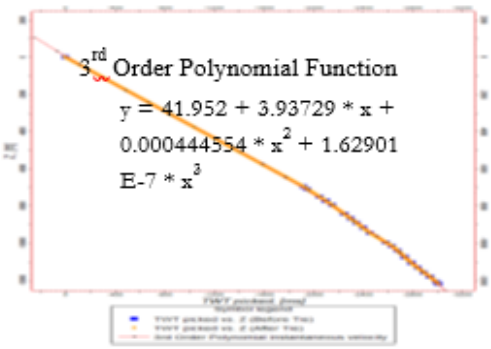

Figure 7. Third Order Polynomial Velocity model Utilized for Converting Reservoir Surfaces from Time to Depth

Middle East Journal of Applied Science & Technology (MEJAST)
Volume 6, Issue 2, Pages 105-117, April-June 2023

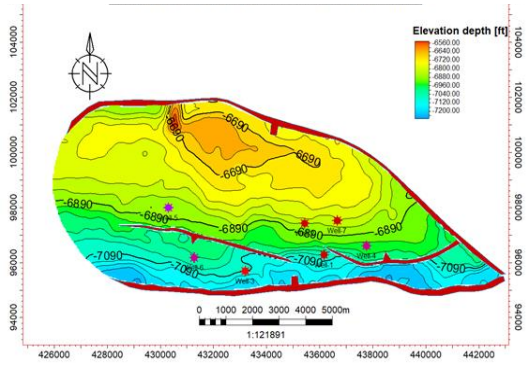

Figure 8. Depth Converted Reservoir Surfaces Using the 3rd Order Polynomial Velocity Function for Reservoir A

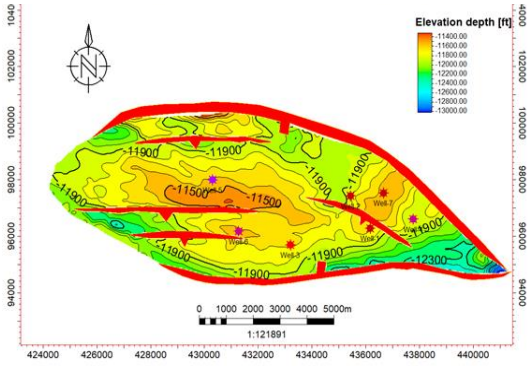

Figure 9. Depth Converted Reservoir Surfaces Using the 3rd Order Polynomial Velocity Function for Reservoir I

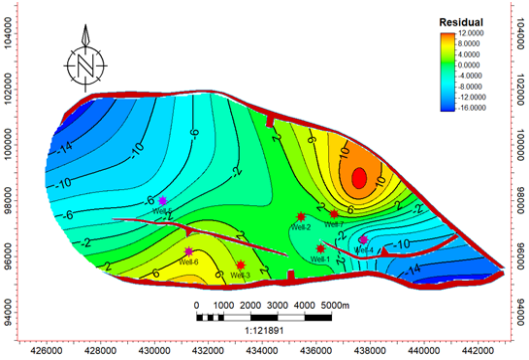

Figure 10. Depth Residual Maps Generated from Surfaces Converted Using the 3rd Order Polynomial Velocity Function for Reservoir A

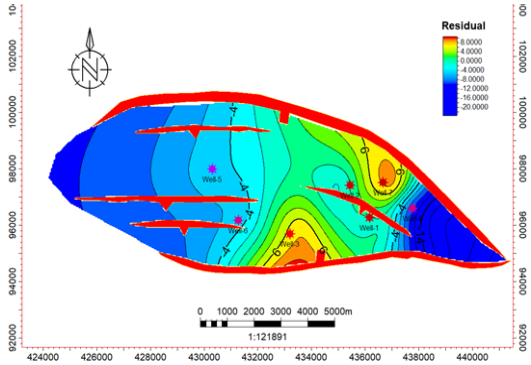

Figure 11. Depth Residual Maps Generated from Surfaces Converted Using the 3rd Order Polynomial Velocity Function for Reservoir I

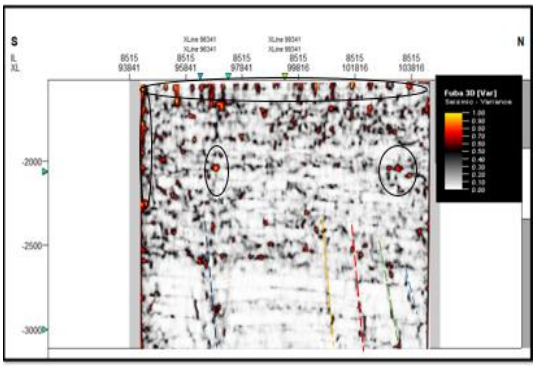

Figure 12. Variance Edge inline 8515

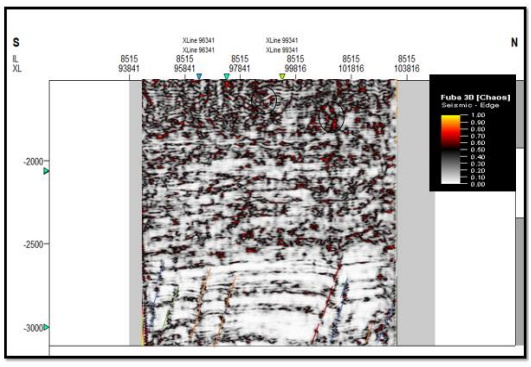

Figure 13. Chaos inline 8515

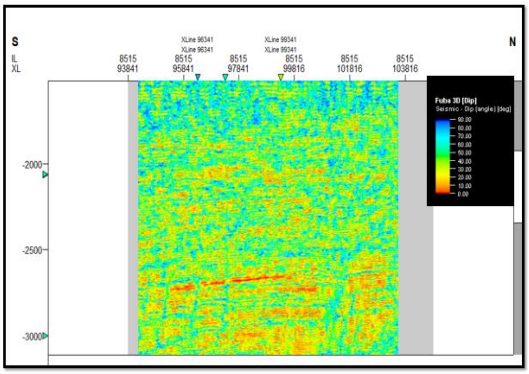

Figure 14. Dip Magnitude Inline 8515

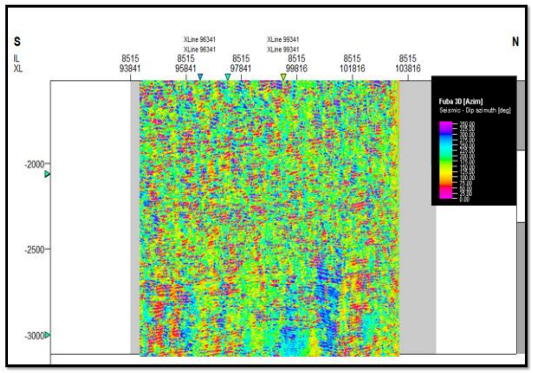

Figure 15. Dip Azimuth Inline 8515

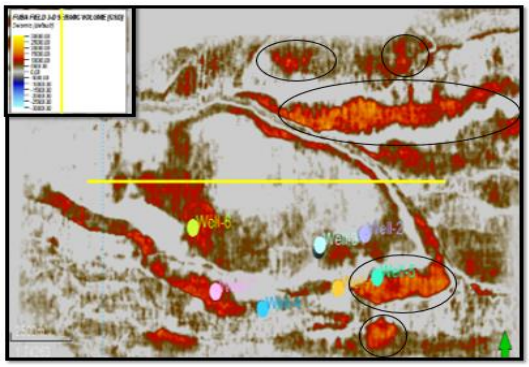

Figure 16. The General Spectral Decomposition Volume at Frequency of 12-35Hz

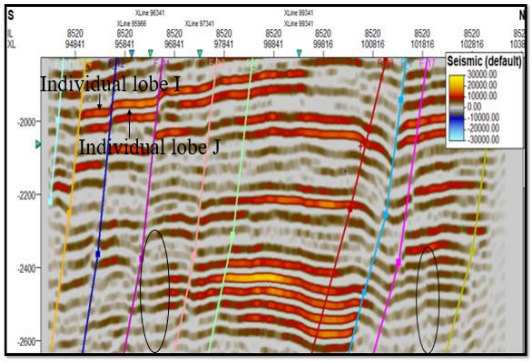

Figure 17. The General Spectral Decomposition at Frequency of 12-35Hz Inline 8820

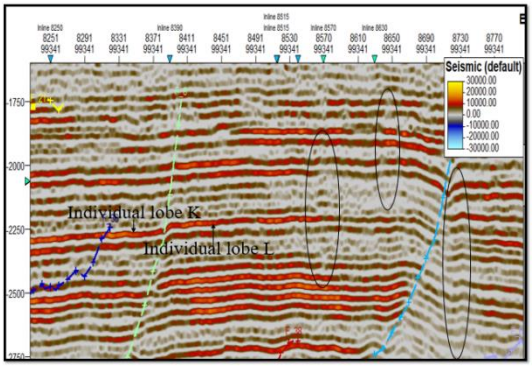

Figure 18. The General Spectral Decomposition at Frequency of 12-35Hz Crossline 99341

4.4. Variance (Edge Detection) Method and Chaos

Figure 12 shows the computed variance attributes of the seismic section while Figure 13 shows the computed chaos attributes. The variance and the chaos values range from 0.0 to 1.0. Values of variance equal to 1 represent discontinuities while a continuous seismic event is represented by the value of 0. The high values are denoted with red to yellow colorations.

On the variance map and the chaos map, the areas dotted with blue, green, orange and pink colored lines signify values that correspond to the location of the discontinuity. The discontinuities may be interpreted as faults and boundaries as shown by the lines drawn on both attribute maps (Law and Chung, 2006). Both the variance edge and the chaos enhanced the faults or sedimentological bodies within the seismic data volume but the chaos enhanced the faults more. Furthermore, several bright spots are also delineated (in black circles and black ovals) which indicate high reflectivity sediments compared to their surroundings. These bright spots are an indication that a potential hydrocarbon trap might exist in the area. The darkest regions in the seismic section, which make vertical strips, may be interpreted as faults or fractures. The zones with low variance and chaos values are due to similar seismic traces. Areas with red patches represent lineaments/discontinuities while grey areas represent the structural framework of the field.

4.5. Dip magnitude and Azimuth

Figures 14 and 15 show the dip and azimuth of the faults. The dip magnitude values range from 0 to 90 while the azimuth values range from 0 to 360. On Figure 14, the green colors represent areas of greater dip, while the red colors represent areas of shallower dip. On Figure 15, blue and orange colors represent opposite dip directions.

4.6. Spectral Decomposition

The general spectral decomposition was done at a frequency of 12-35Hz. Figure 16 is the seismic volume obtained. Figure 16 illustrates Red-Green-Blue blend of the higher resolution of the frequency of 12-35Hz. The RGB colour blend effect gives a better understanding of the geology reservoirs. The colour blend is spectral balancing which recompense for wavelet and energy loss. The figure showed a complex meandering system and other less winding channels which are discontinuous and difficult to resolve on the seismic. In this figure, the areas in red color indicate areas of low frequency and high amplitude associated with known hydrocarbon zones and when one colour is dominating, it showed that the frequency is dominating at that point. It revealed the geometry of the channels and other fewer sinusoidal channels. The channels are displayed with bright colouration which contains multiple frequencies as observed within the low frequency areas and indicated in black circles and ovals. The meandering channels run across from the north-eastern to the south-eastern part. These are likely traps for hydrocarbon accumulation (Neuendorf, et al, 2005). The amplitude response which is dominated by blue colour is high frequency. At the central part, there is high amplitude, an indication of hydrocarbon/gas effect. At parts where there's a change in colour to brownish, it showed thickening up of the reflectors and greater contribution from the lower frequencies. There are colour changes in the channel system which could be indicative of changes in lithology. As can be seen in the areas in black ovals in the figures 17 and 18, the results of spectral decomposition at this frequency indicates there is continuity of faults and the presence of small scale faults in the field.

4.7. Stratigraphic Contact

A major geologic feature was observed on the time-slice from the divergent pattern on the seismic section as we penetrate deeper, which is an unconformity (Figures 17 and 18). This represents a significant break in vertical velocity or breaks in deposition time or record on horizon (Neuendorf, et al, 2005). This type of unconformity is called angular unconformity. Angular unconformity is an unconformity between two groups of rocks whose bedding planes are not parallel or in which the older underlying rock dips at a different angle (usually steeper) than the younger, overlying strata. Its interpretation depends on the recognition of characteristic reflection geometries rather than on amplitude information. It shows that deposition of the sediments took place at different times. Some of the lobes are indicated in Figures 17 and 18 (individual lobes I, J, K and L).

As can be seen in the areas in black ovals in Figures 17 and 18, the results of spectral decomposition at frequencies between 12Hz and 35Hz indicate the following: (a) There is more continuity of faults than previously interpreted; (b) The presence of small scale faults in the field.

Table 1. Depth Residual between Well Tops and Resultant Depth Surfaces

Reservoir/ Well	**Well Top (ft)**	**Depth Surface (ft)**	**Difference (ft)**	**Depth Surface (ft)**	**Difference (ft)**	**Depth Surface (ft)**	**Difference (ft)**
		Linear Velocity Function		***2nd Order Polynomial***		***3rd Order Polynomial***	
Reservoir A Well-1	-7054.07	-7079.08	25.01	-7032.58	-21.49	-7053.13	-0.95

Well-2	Missing	Missing	Missing	Missing	Missing	Missing	Missing
Well-3	-6877.06	-6849.08	-27.98	-6886.40	9.34	-6880.86	3.80
Well-4	-6977.93	-7039.60	61.67	-7004.73	26.80	-6971.24	-6.69
Well-5	-6905.39	-6873.79	-31.60	-6859.58	-45.81	-6900.65	-4.74
Well-6	-7065.18	-7105.10	39.92	-7028.91	-36.27	-7070.87	5.69
Well-7	-6846.24	-6877.44	31.20	-6854.65	8.41	-6852.85	6.61
Reservoir I Well-1	-11690.91	-11720.12	29.21	-11674.22	-16.69	-11690.91	0.00
Well-2	-11823.41	-11780.54	-42.87	-11807.54	-15.87	-11823.41	0.00
Well-3	-11650.06	-11684.44	34.38	-11666.36	16.30	-11656.67	6.61
Well-4	-11887.08	-11845.26	-41.82	-11912.42	25.34	-11877.60	-9.48
Well-5	-11599.86	-11549.01	-50.85	-11581.29	-18.57	-11595.11	-4.75
Well-6	-11569.00	-11534.94	-34.06	-11586.60	17.60	-11564.27	-4.73
Well-7	-11551.91	-11592.75	40.84	-11534.64	-17.27	-11560.33	8.42

5.0. Conclusion

A total of nine sand bodies (A, B, C, D, E, F, G, H, I) were identified and correlated across all seven wells in the field. Two horizons (A and I) were selected for the study. Structural analysis of the field revealed that reservoir A and I are anticlinal structures supported by two major bounding faults. Structural interpretation of seismic data revealed that the field is highly faulted with synthetic and antithetic faults which are in line with faults trends identified in the Niger Delta. All interpreted faults are normal synthetic and antithetic faults. A total of twenty-nine faults were interpreted across the entire seismic data. Of the 29 interpreted faults, only F1 (synthetic fault) and F16 (antithetic fault) faults are regional, running from the top to bottom across the field.

Hence, these faults play significant roles in trap formation at the upper, middle and lower sections of the field. Fault and horizon interpretation revealed that closures found on A and I reservoirs are collapsed crestal structures bounded by the two major faults. The depth structure maps reveal that the reservoirs are anticlinal and fault supported. Reservoir A is found at a shallower depth from 6500 to 7500ft while reservoir I is found at a deeper depth ranging from 11500 to 13000ft respectively. The synthetic and antithetic faults act as good traps for the hydrocarbon accumulation in the study area. The variance and chaos attributes values range from 0.00 to 1.00. They revealed the subtle structures and faults in the seismic section. The variance and chaos attributes analysis in this study have helped in increasing the understanding of the delineated reservoirs and geological structures in the study area towards a better delineation of hydrocarbon potential and improved reservoir characterization. The dip magnitude and azimuth values range from 0 to 90 degrees and 0 to 360 degrees.

The results of spectral decomposition at a frequency of 12-35Hz indicates areas of low frequency and high amplitude associated with known hydrocarbon zones, there is continuity of faults and the presence of small scale faults, lobes and channels in the field. Furthermore, it has been demonstrated that seismic attributes are complementary to the information derived through traditional methods of seismic interpretation. In reservoirs, hydrocarbons were encountered by all seven wells drilled in the field. Finally, it is recommended that further studies should be done on the mapping of thin sandstone reservoirs in the study area.

Declarations

Source of Funding

This study did not receive any grant from funding agencies in the public or not-for-profit sectors.

Competing Interests Statement

The author has declared no competing interests.

Consent for Publication

The author declares that she consented to the publication of this study.

Acknowledgments

The author is grateful to Shell Petroleum Development Company of Nigeria (SPDC), Port Harcourt Nigeria for the release of the academic data for the purpose of this study.

References

[1] Liner, C.L. (2004). Elements of 3D Seismology, 2nd Edition, Penn Well Books, Tulsa, OK.

[2] Oyeyemi, K.D. & Aizebeokhai, A.P. (2015). Seismic Attributes Analysis for Reservoir Characterization; Offshore Niger Delta. Petroleum and Coal, 57(6): 619–628.

[3] Adewoye, O., Amigun, J.O. & Afuwai, C.G. (2015). Lithostratigraphic Interpretation and Seismic Attributes Analysis for Reservoir Characterization in Some Parts of Niger Delta. Petroleum and Coal, 57(1): 76–84.

[4] Steiner, W. & Lockhart, J. (1988). Seismic Classification and Reservoir Volume Analysis of the Upper Wahoo Oil Field, www.petrobjects.com/papers.

[5] Adetokunbo, P., Al-Shuhail, A.A., & Al-Dossary, S. (2016). 3D Seismic Edge Detection Using Magic Squares and Cubes. Interpretation, 4(3): 271–280.

[6] Emujakporue, O.G. & Enyenihi, E.E. (2020). Identification of Seismic Attributes for Hydrocarbon Prospecting of Akos field, Niger Delta, Nigeria. SN Applied Sciences, 2: 910.

[7] Ologe, O. & Olowokere, T.M. (2021). Seismic Attributes Analysis as a Precursor to Hydrocarbon Indicators: A Case Study of "Ok" Field, Niger Delta. Tanzania Journal of Science, 47(1): 134–144.

[8] Srivastava, A.K., Singh, V., Samanta, B.G. & Sen, G. (2003). Utilization of Seismic Attributes for Reservoir Mapping: A Case Study from Cambay Basin, India. CSEG Recorder, 28(8): 46–50.

[9] Ochoma, U, Tamunobereton-ari I., Amakiri, A.R.C. Sigalo, F.B. & Horsfall O.I. (2023). 3-D Seismic Attributes Analysis for Enhanced Hydrocarbon Prospect Definition of Onshore Fuba Field Niger-Delta, Nigeria. IOSR Journal of Applied Geology and Geophysics, 11(2): 63–70.

[10] Omoja U.C. & Obiekezie T.N. (2019). Application of 3D Seismic Attribute Analyses for Hydrocarbon Prospectivity in Uzot-Field, Onshore Niger Delta Basin, Nigeria. International Journal of Geophysics, Pages 1–11.

[11] Whiteman, A. (1982). Nigeria: Its Petroleum Ecology Resources and Potential. London, Graham and Trotman.

[12] Adegoke, O.S., Oyebamiji, A.S., Edet, J.J, Osterloff, P.L. & Ulu, O.K (2017). Cenozoic Foraminifera and Calcareous Nannofossil Biostratigraphy of the Niger Delta. Elsevier, Cathleen Sether, United States.

[13] Short, K.C. & Stable A.J. (1967). Outline of Geology of Niger Delta. Bulletin of America Association of Petroleum Geologists, 51(5): 761–779.

[14] Horsfall, O.I., Uko, E.D., Tamunoberetonari I. & Omubo-Pepple, V.B. (2017). Rock-Physics and Seismic-Inversion Based Reservoir Characterization of AKOS FIELD, Coastal Swamp Depobelt, Niger Delta, Nigeria. IOSR Journal of Applied Geology and Geophysics, 5(4): 59–67.

[15] Ochoma, U., Uko E.D. & Horsfall, O.I. (2020). Deterministic hydrocarbon volume estimation of the Onshore Fuba Field, Niger Delta, Nigeria. IOSR Journal of Applied Geology and Geophysics, 8(1): 34–40.

[16] Pigott. J.D., Kang, M.I.H. & Han, H.C. (2013). First Order Seismic Attributes for Clastic Seismic Facies Interpretation: Examples from the East China Sea. Journal of Asian Earth Science, 66: 34–54.

[17] Cohen L. (1989). Time-frequency Distributions-a Review. Proc. IEEE, Pages 941-981.

[18] Ogbamikhumi, A. & Aderibigbe, T.O. (2019). Velocity Modelling and Depth Conversion Uncertainty Analysis of Onshore Reservoirs in the Niger Delta Basin. J of the Cameroon Academy of Sciences, 14(3): 239–247.

[19] Law W.K. & Chung A.S.C. (2006). Minimal Weighted Local Variance as Edge Detector for Active Contour Models. In: Narayanan et al. PJ (Eds), Accv 2006, LNCS 3851, Pages 622–632.

[20] Neuendorf, K.K.E., Mehl, J.P. & Jackson, J.A. (2005). Glossary of Geology, Fifth Edition. American Geological Institute, Alexandria, Virginia, Page 779.